Supporting Information

High-throughput concentration of rare malignant tumor cells from large-volume effusions by multistage inertial microfluidics

Nan Xiang* and Zhonghua Ni
School of Mechanical Engineering, and Jiangsu Key Laboratory for Design and Manufacture of Micro-Nano Biomedical Instruments, Southeast University, Nanjing, 211189, China.
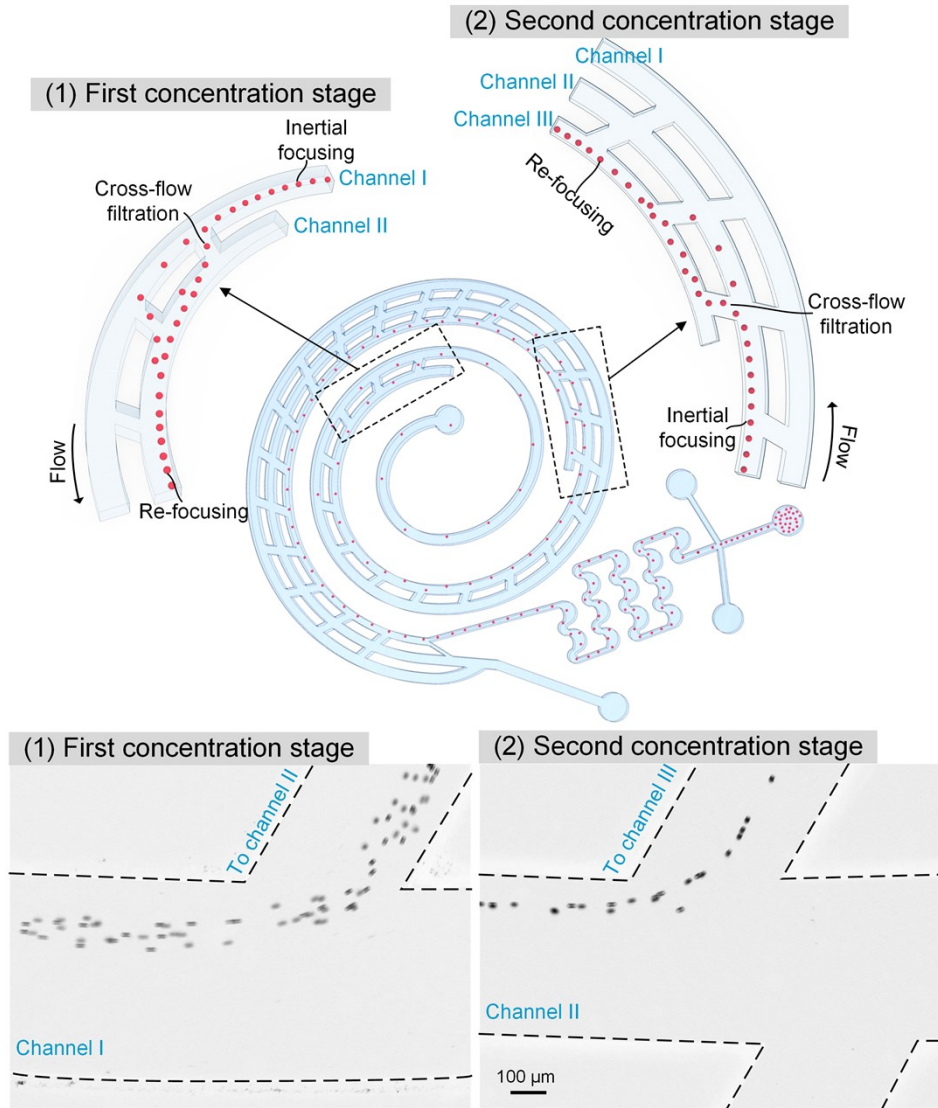**nan.xiang@seu.edu.cn. Tel: +86 (025) 52090508.*

Figure S1. Diagram and experimental results illustrating the cell migration in (1) first concentration stage and (2) second concentration stage. The black dotted lines in the composite images mark the channel walls. The cells are first focused into a train near the inner channel wall (inertial focusing of cells) under the balance of the inertial lift force (F_L) directing toward the channel wall and the Dean drag force (F_D) directing toward the channel centerline. The inertial lift force (F_L) is actually a net force of the shear-induced inertial lift force (F_{LS}) moving cells toward the channel wall and the wall-induced inertial lift force (F_{LW}) pushing cells away from the channel wall. When reaching the transversal cross-flow channels, the cells will flow into the transversal cross-flow channels due to the curved streamlines and the disappearance of wall-induced inertial lift force (F_{LW}) and Dean drag force (F_D). Multiplexing transversal cross-flow channels were designed along the channel length to ensure efficient cell transfer. Commonly, the cells could be completely transferred into the inner channel through using less than three cross-flow channels. After being transferred from channel I into channel II, the steps of inertial focusing and cross-flow filtration are repeated. Finally, the cell train will be transferred into the channel III, leaving the cell-free fluids in channels I and II.
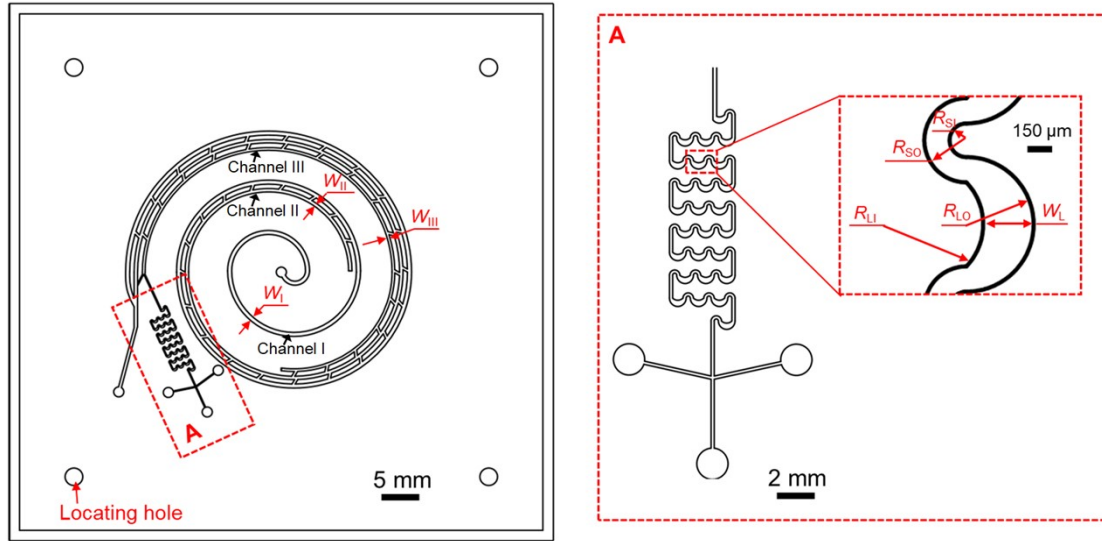
Figure S2. CAD drawing of the microfluidic concentrator. The channel widths of channels I, II, and III were W_I, W_{II}, and W_{III}, respectively. The neighboring channels were connected with each other by multiplex transversal cross-flow channels with a channel width of $W_C = 400$ μm and a channel length $L_C = 800$ μm (the angle between the cross-flow channel and the main channel was 60° and the arc length between the adjacent cross-flow channels was 4.25 mm). Four locating holes were designed to assist the assembly of multiplex layers. The magnified region A shows the detailed structure of the bended asymmetric serpentine channel. Each unit of the serpentine channel consists of a large curving turn (with an inner radius of $R_{LI} = 360$ μm, an outer radius of $R_{LO} = 400$ μm, and a maximum turn width of $W_L = 300$ μm) and a small curving turn (with an inner radius of $R_{SI} = 100$ μm, an outer radius of $R_{SO} = 250$ μm, and a constant turn width of $W_S = 150$ μm). By calculating the required channel length for achieving the inertial cell focusing under the flow rate of 200 μL/min, the number of the repeated serpentine units were determined to be 25.
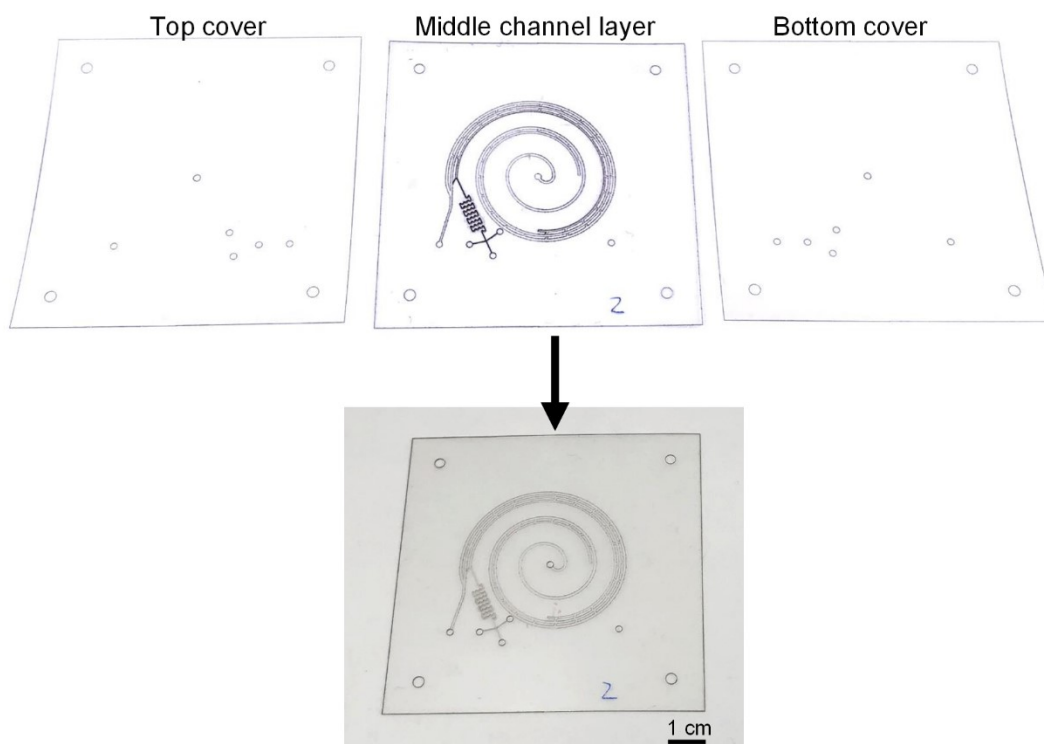
Figure S3. Photographs of the three layers of polymer films for fabricating the single device. The single device was assembled with three layers of polymer films: one top cover, one middle channel layer, and one bottom cover. The bottom row shows the photograph of the fabricated single device.
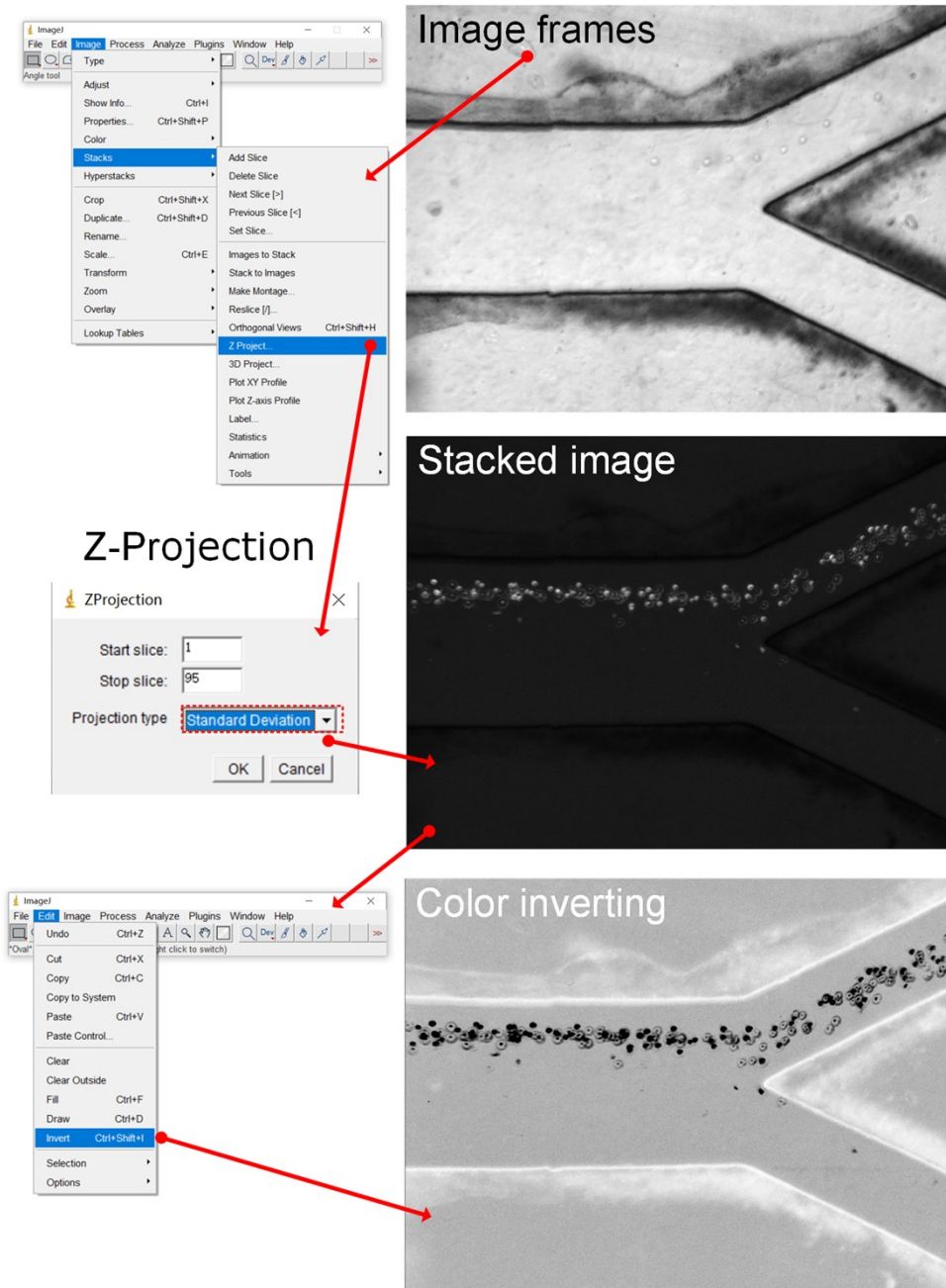
Figure S4. Image processing procedure for creating the composite images illustrating the cell distributions. Image frames captured over a certain time period were stacked using the Z projection option (with the projection type of 'standard deviation') of ImageJ software (https://imagej.nih.gov/ij/) to create stacked composite images. To clearly illustrate the statistical cell distribution, the color of the composite image was inversed using the ImageJ software.
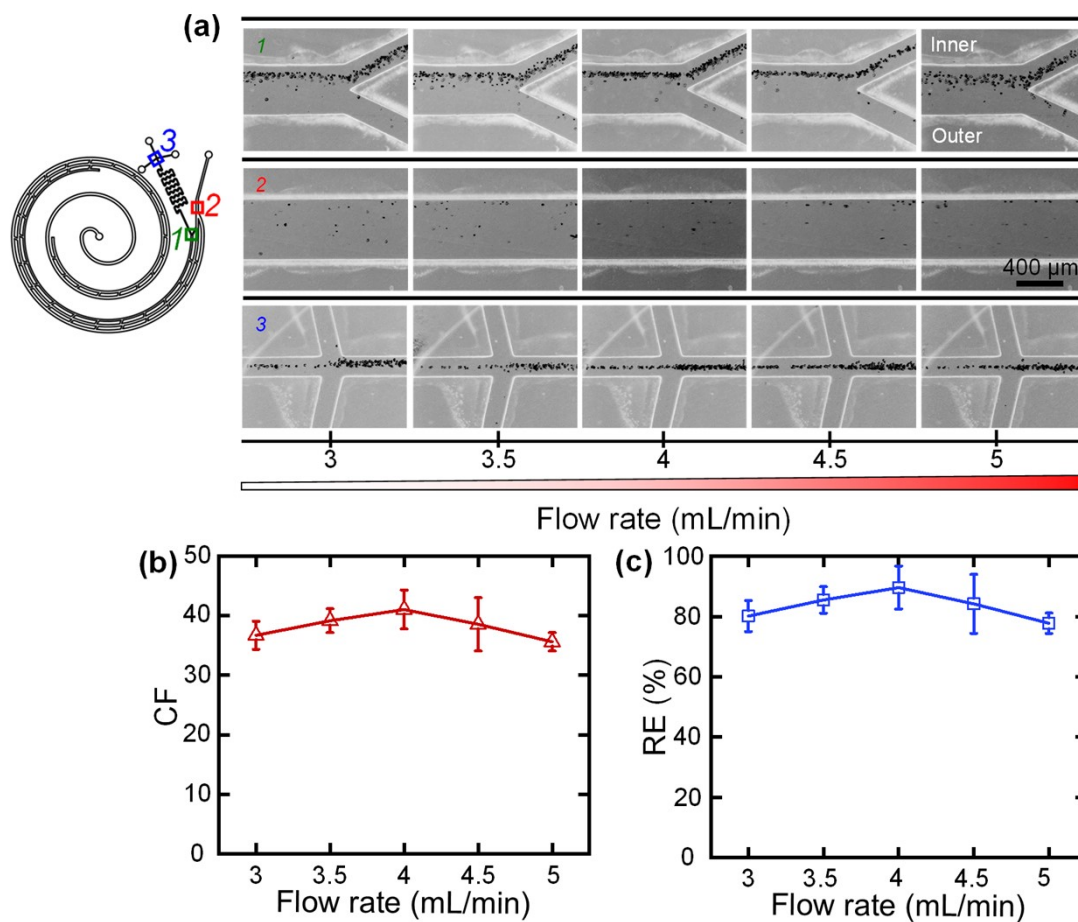
Figure S5. (a) Composite images illustrating the distributions of MCF-7 cells at selected positions: 1, Y-shaped outlet at the end of channel III; 2, waste fluid channel; and 3, cross-shaped outlet at the end of serpentine channel; at variable flow rates (3–5 mL/min) with an interval of 0.5 mL/min. **(b)** Concentration factor (CF) of MCF-7 cells at variable flow rates. **(c)** Recovery ratio (RE) of MCF-7 cells at variable flow rates.
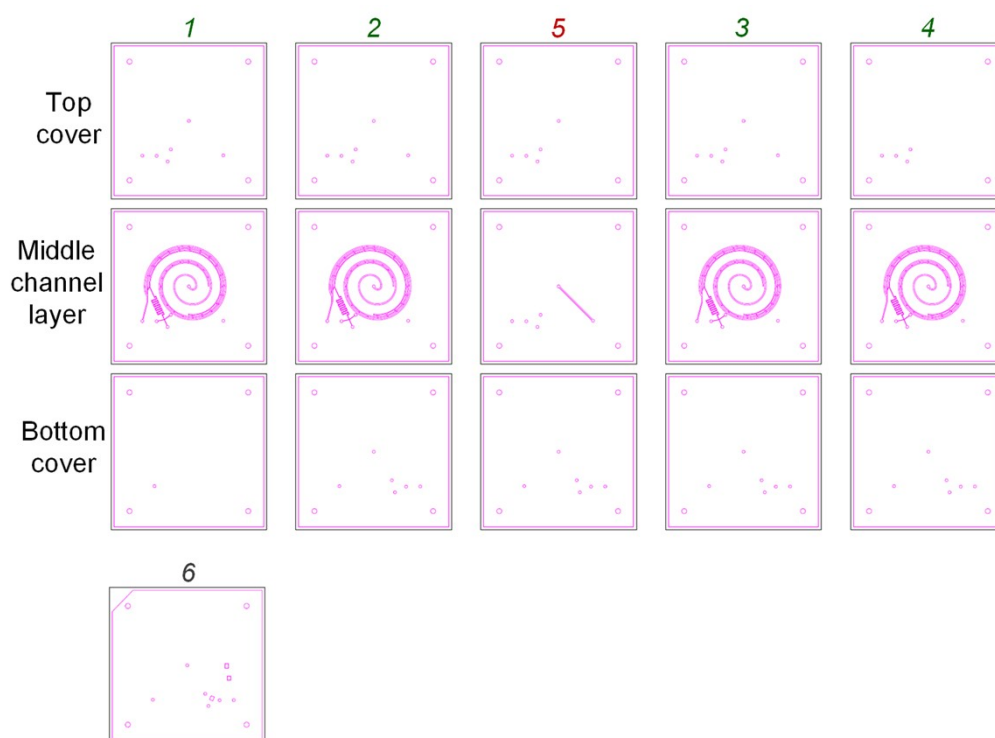
Figure S6. CAD drawings of each layer (1-6) for fabricating the multiplexed device. Each channel layer (1-5) was fabricated with three layers of polymer films: one top cover, one middle channel layer, and one bottom cover). The double-sided tape (6) was used to bond different channel layers.
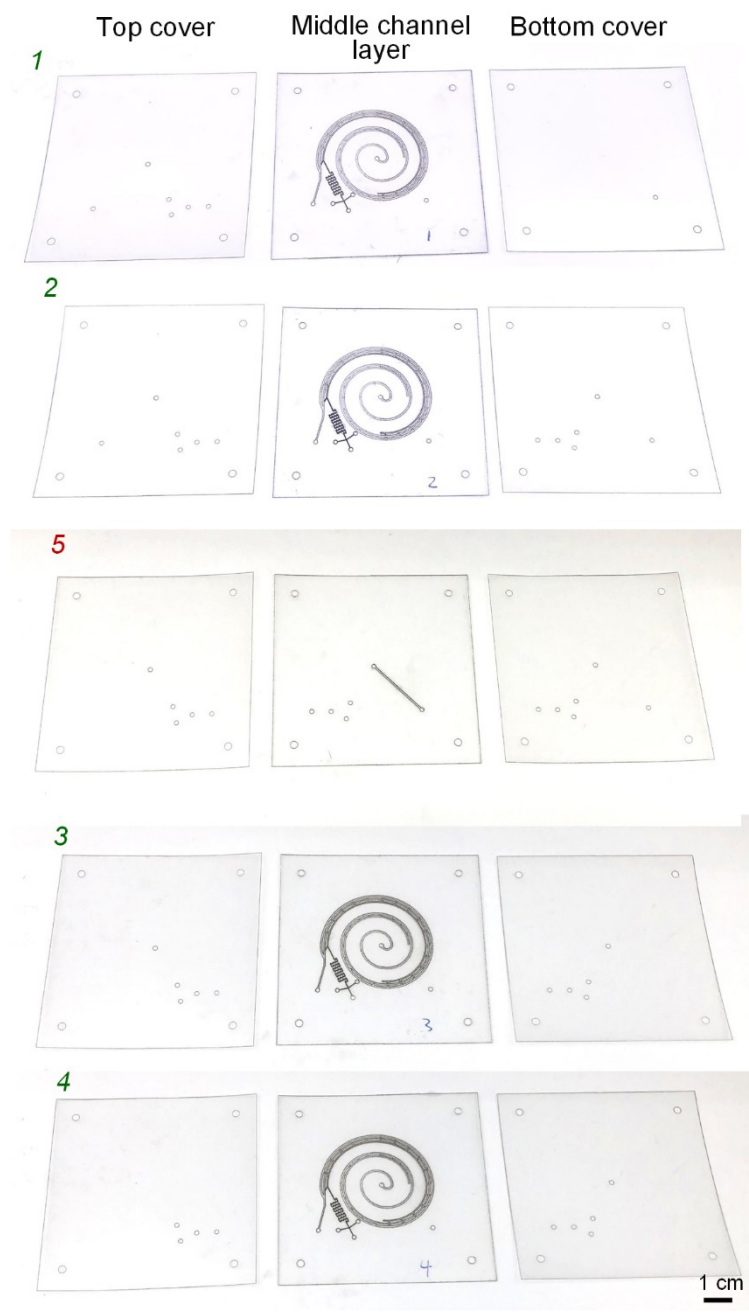
Figure S7. Photograph of each channel layer (1-5) for fabricating the multiplexed device. Each channel layer (1-5) was fabricated with three layers of polymer films: one top cover, one middle channel layer, and one bottom cover.
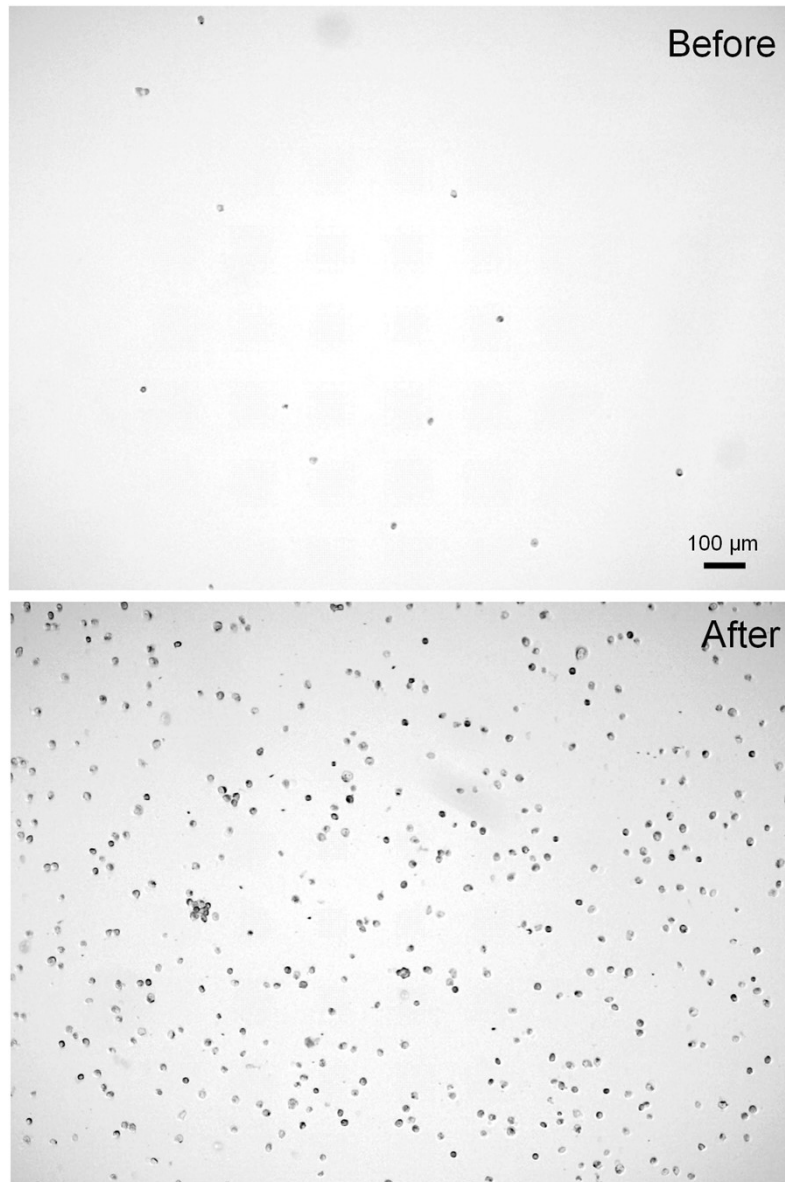
Figure S8. Microscopic images of the samples before and after concentration. The A549 cell suspension prepared with a low initial concentration of 8.8×10^4 counts/mL (the upper microscopic image) was pumped into the multiplexed device at an ultrahigh throughput of 16 mL/min, and the samples collected from the target outlet were illustrated in the lower microscopic image. This figure is the magnified version of Figure 3(f).
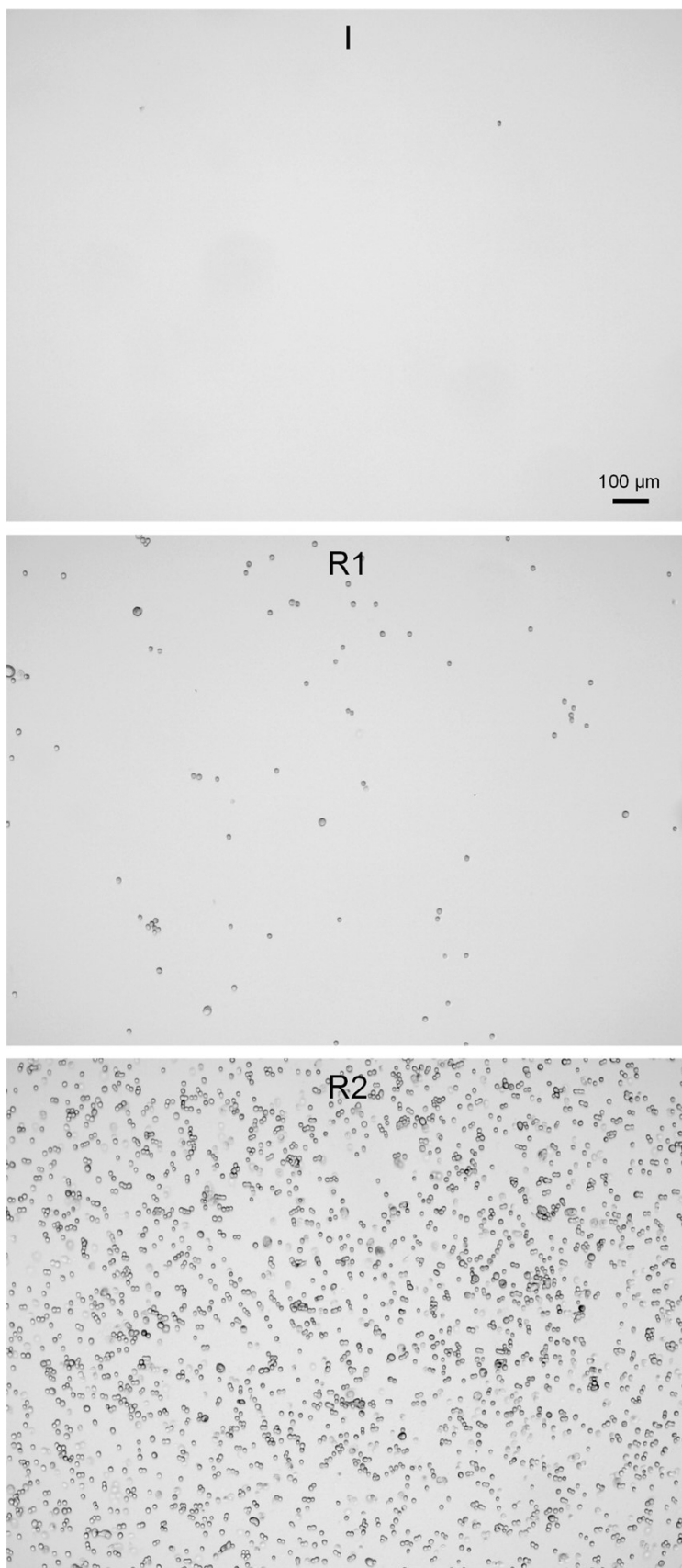
Figure S9. Microscopic images of the initial sample (I) and the target samples collected after each run step (R1 and R2). This figure is the magnified version of Figure 4(b).

Supplementary video S1. A video illustrating the migration dynamics of A549 cells at the Y-shaped outlet at the end of channel III at the optimal flow rate of 4 mL/min.

Supplementary video S2. A video illustrating the migration dynamics of A549 cells at the waste fluid channel at the optimal flow rate of 4 mL/min.

Supplementary video S3. A video illustrating the migration dynamics of A549 cells at the cross-shaped outlet at the end of serpentine channel at the optimal flow rate of 4 mL/min.